

Numerical Characterization and Optimization of the Microfluidics for Nanowire Biosensors

Dong Rip Kim and Xiaolin Zheng*

Department of Mechanical Engineering, Stanford University,
Stanford, California 94305

Received June 1, 2008; Revised Manuscript Received August 2, 2008

ABSTRACT

The present study aims to enhance the analyte transport to the surface of nanowires (NWs) through optimizing the sensing configuration and the flow patterns inside the microfluidic channel, and hence to reduce the response time of NW biosensors. Specifically, numerical simulations were carried out to quantitatively investigate the effects of the fundamental surface reaction, convection, and diffusion processes on the sensing performance. Although speeding up all these processes will reduce the sensing response time, enhancing the diffusional transport was found to be most effective. Moreover, the response time of NW biosensors is inversely proportional to the local concentration of the analyte in the vicinity of the NWs, which suggests that the sensing response time can be significantly reduced by replenishing the local analyte rapidly. Therefore, the following three optimization strategies were proposed and their effects on the time response of NWs were characterized systematically: device substrate passivation, microfluidic channel modification, and suspending NWs. The combination of these three optimization methods was demonstrated to be able to reduce the response time of NW biosensors by more than 1 order of magnitude.

Semiconductor nanowire biosensors, configured as field effect transistors (FET), are emerging as a powerful platform for direct detection of biological and chemical species.¹⁻⁶ Significantly, nanowires (NWs), particularly silicon nanowires (SiNWs), have been successfully demonstrated as real-time, label-free, multiplexing, and femtomolar level accuracy biosensors in detecting a range of species, including proteins, viruses and DNAs.¹⁻⁷ Although the SiNW biosensors have reached the femtomolar level of sensitivity,⁴⁻⁶ there is still room for further improvement in terms of the sensitivity and especially the detection time. Nanowire biosensing experiments are typically conducted in a rectangular microfluidic channel with the NW biosensors placed on the floor of the channel where the local convection velocity is almost zero.⁸ The inefficient mass transport of the analyte to the biosensors limits the further improvement of the sensitivity and the detection time of the NW biosensors.⁹⁻¹¹ The effect of analyte transport on the biosensors has been quantified through theoretical and numerical studies,⁹⁻¹⁴ but the analyte surface binding reactions have frequently been assumed to be infinitely fast^{9,11} with the result that the coupling between the mass transport and surface binding reactions is lacking.

The importance of analyzing the coupling between diffusion, convection, and reaction was also pointed out by a very

recent publication by Squires et al.¹⁵ They provided intuitive understanding of the competing processes by discussing extreme conditions, such as when the convection velocity is zero or when the surface binding reaction is infinite fast. However, the NW biosensors frequently do not operate at these extremes so analysis using detailed experimental parameters is needed for more quantitative understanding and predictions of these sensing systems. Moreover, only limited effort⁷ has been devoted to optimizing the microfluidics at the NW biosensing site to enhance the analyte transport. Here, we first quantify the individual and coupled effects of convection, diffusion, and surface binding reactions on the sensing performance of the NW biosensors through numerical simulation using detailed experimental parameters, and then propose and characterize three simple strategies to improve the sensitivity and reduce the detection time of the NW biosensors.

The numerical simulation schematic was set up on the basis of the reported experimental configuration (Figure 1a),⁸ where a 2 μm long NW is located at the center of the floor of a microfluidic channel (LWH: 1 mm \times 500 μm \times 50 μm). The sensing system was simplified into a two-dimensional problem by focusing only on the axial cross-section of the channel (Figure 1b). Although a full three-dimensional simulation would be more accurate, the qualitative trends will be the same.

* To whom correspondence should be addressed. E-mail: xlzheng@stanford.edu.

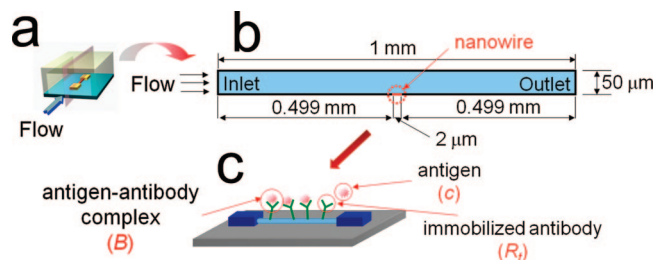


Figure 1. Schematic of the numerical setup. (a) The NW biosensor is located at the center of the floor of the microfluidic channel. (b) The cross-section of the microfluidic channel with a 2 μm long NW in the bottom wall center, parallel to the flow. (c) Schematic of the surface binding reaction on the NW, where the antigen c binds to the immobilized antibody R_t , forming the antigen–antibody complex B .

The binding reaction between the immobilized antibody R_t (mol m^{-2}) and the targeted antigen c (mol m^{-3}) is described by a one-step, reversible surface reaction¹²



$$\frac{\partial B}{\partial t} = k_a c (R_t - B) - k_d B \quad (2)$$

where B is the bound antigen–antibody complex (mol m^{-2}) (Figure 1c), k_a is the association rate constant ($\text{M}^{-1} \text{s}^{-1}$), and k_d is the dissociation rate constant (s^{-1}). The conductance of NW FET biosensors changes in response to the net bound charge, which is proportional to the concentration of complex B . Therefore, the sensing performance of NWs can be represented by the dynamics of the concentration of complex B (eq 2). Specifically, the equilibrium concentration of complex B_{eq} corresponds to the ultimate sensitivity. The concentration of complex B and the complex formation rate dB/dt indicate the signal magnitude and rate of signal rise, respectively, so they are adopted here to characterize the sensing response time.

The spatial and temporal variations of the antigens inside the microfluidic channel are described by the convection-diffusion equation

$$\frac{\partial c}{\partial t} + \vec{u} \cdot \nabla c = D \nabla^2 c \quad (3)$$

where u is the flow velocity (m s^{-1}), and D is the diffusion coefficient of the antigen in the analyte solution ($\text{m}^2 \text{s}^{-1}$). The flow velocity field inside the microfluidic channel is described by the continuity (eq 4) and Navier–Stokes equations (eq 5)

$$\nabla \cdot \vec{u} = 0 \quad (4)$$

$$\frac{\partial \vec{u}}{\partial t} + \vec{u} \cdot \nabla \vec{u} = -\frac{\nabla p}{\rho} + \frac{\mu}{\rho} \nabla^2 \vec{u} \quad (5)$$

where p is pressure (N m^{-2}), ρ is density (kg m^{-3}), and μ is the dynamic viscosity (Pa s). The following assumptions were made in our calculations: (1) the flow is incompressible with constant properties due to small Reynolds number (~ 0.1), (2) the analyte distribution does not affect the flow velocity field, and (3) the bulk fluid is electro-neutral, and the electrokinetic effects are negligible inside the thin electric double layer. The parameters used for the calculations are summarized in ref 16.

To solve the above governing equations (eqs 2–5), the boundary conditions are specified as follows:

	Velocity	Analyte
Inlet:	parabolic velocity profile	$c = c_0$
Outlet:	straight-out	$\vec{n} \cdot (D \nabla c) = 0$
Wall (except NWs):	no-slip	$\frac{\partial c}{\partial \vec{n}} = 0$
NW surface:	no-slip	$D \nabla c = \frac{\partial B}{\partial t}$

(6)

where \vec{n} is the unit normal vector to the surface. Moreover, the velocity \vec{u} and concentrations of c and B were set to be zero at $t = 0$, as initial conditions. The simulations were carried out using FEMLAB™ software (Comsol, Stockholm, Sweden). The same governing equations and boundary conditions were also used by several previous studies^{12,13,15} and the accuracy of the simulation was validated²¹ by duplicating the published calculation results of similar problems.^{12,13}

The effects of the convection and diffusion-driven transport of analyte on the sensing performance are illustrated in Figure 2a,b, respectively. First, for both convection and diffusion, the complex formation rate dB/dt increases more rapidly with increasing the inlet velocities and diffusion coefficients when they are small and become less sensitive at higher velocity and diffusion coefficient. When the inlet velocity and diffusion coefficient are low, the surface binding reaction is relatively fast, so the sensing is transport limited. In contrast, when the inlet velocity and diffusion coefficient are high, the surface binding reaction becomes the slow process, so that the sensing response time is limited by reaction kinetics. These observations are consistent with previous studies.^{12,15,23} Specifically, the typical protein sensing conditions^{1,8,22} (flow velocity $u_0 = 1.7 \text{ mm s}^{-1}$ and diffusion coefficient $D = 6 \times 10^{-11} \text{ m}^2 \text{ s}^{-1}$), marked as the dashed lines in Figure 2a,b, fall into the transport-limited region, confirming the deficiency in the analyte mass transport. Second, the relative rates of the surface reaction and the diffusional transport can be described by the nondimensional Damköhler number $\text{Da} = k_a R_t H / D$, where H is the characteristic length and is equal to half of the channel height of $50 \mu\text{m}$. The Da number for the current protein system is about 34 ($\gg 1$), indicating that diffusion is a much slower process than reaction.¹⁵ The relative rate of the convective and diffusional transport in the mass transfer layer next to the NW surface is represented by the nondimensional shear Péclet number $\text{Pe}_s = u_0 L^2 / HD$,^{11,15} where L is the length of NW. The Pe_s number for the current protein system is about 4.53, which implies that the diffusional transport is slightly slower than the convective transport, as well. Moreover, as shown in Figure 2a,b, the complex formation rate dB/dt is proportional to the inlet velocity to the power of 0.16 but to the diffusion coefficient to the power of 0.50. The stronger dependence on diffusion is consistent with the previous asymptotic analysis.¹¹ In summary, diffusion is the slowest process, surface reaction is the fastest, and convection is slightly faster than diffusion.

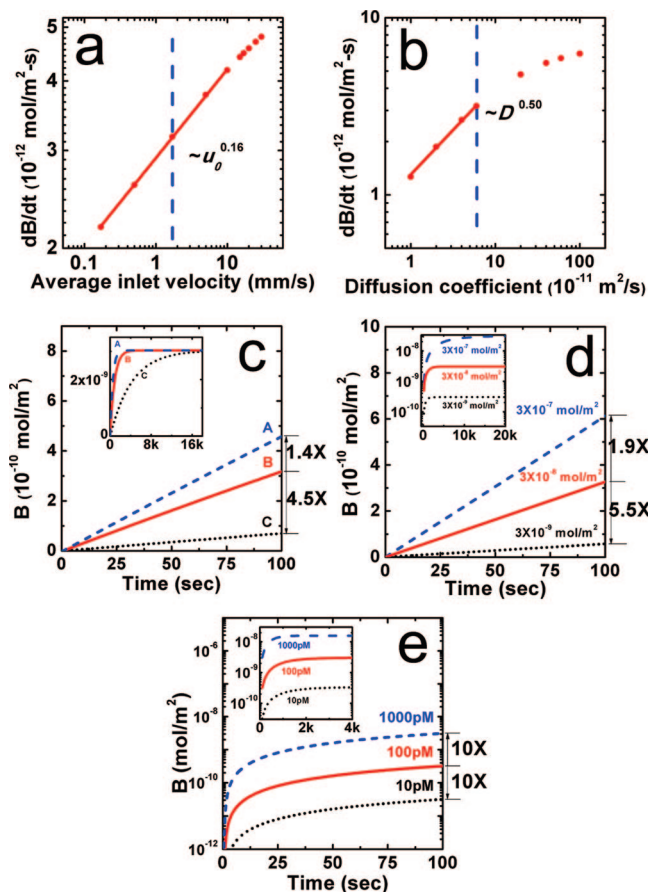


Figure 2. Effects of convection, diffusion, surface reaction, and inlet concentration on the NW sensing performance. (a) Effects of convection on the complex formation rate (log–log plot). dB/dt ($t = 100$ s). (b) Effects of diffusion on the complex formation rate (log–log plot). dB/dt ($t = 100$ s). (c) Effects of the association/dissociation rate constant on the complex concentration under the same affinity constant (A, $k_a = 2.7 \times 10^7 \text{ M}^{-1}\text{s}^{-1}$, $k_d = 2.4 \times 10^{-2} \text{ s}^{-1}$; B, $k_a = 2.7 \times 10^6 \text{ M}^{-1}\text{s}^{-1}$, $k_d = 2.4 \times 10^{-3} \text{ s}^{-1}$; C, $k_a = 2.7 \times 10^5 \text{ M}^{-1}\text{s}^{-1}$, $k_d = 2.4 \times 10^{-4} \text{ s}^{-1}$) such that equilibrium complex concentration remains the same. (d) Effects of the immobilized antibody density on the concentration of complex B . (e) Effects of the inlet concentration on the concentration of complex B . The insets for all the graphs show the long-term response.

We further characterized the effect of the surface binding reaction on the sensing performance. In the one-step binding reaction (eq 2), the equilibrium complex concentration B_{eq} can be expressed as

$$B_{\text{eq}} = \frac{R_t c}{c + (k_d/k_a)} \quad (7)$$

First, the equilibrium complex concentration B_{eq} remains constant for the fixed affinity constant k_a/k_d (Figure 2c, inset), and is linearly proportional to the antibody concentration R_t (Figure 2d, inset) and the antigen concentration c (Figure 2e, inset). Second, when the concentration of antigen c is increased/decreased by a factor of 10, the complex concentration B at $t = 100$ s changes linearly by the same factor (Figure 2e), but only changes by a factor of 1.4/4.5 and 1.9/5.5 as the association rate constant k_a and the antibody density R_t are increased/decreased by a factor of 10 (Figure 2c,d), respectively. This suggests that the antigen is the deficient,

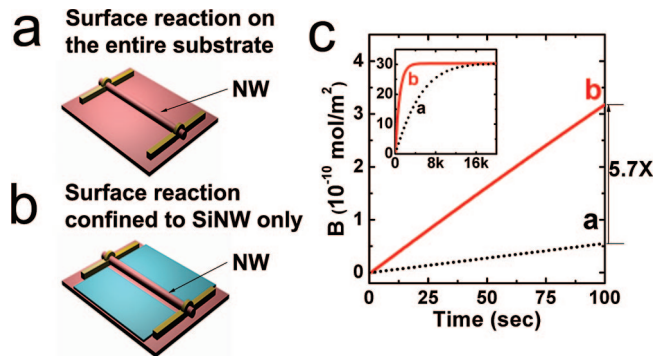


Figure 3. Effect of device substrate passivation on the complex formation rate. (a) Normal SiNW biosensor on the silicon substrate: surface reaction occurring on the entire substrate. (b) Blocking the surface reaction on the substrate by passivating the substrate: surface reaction confined to SiNW only. (c) The binding rate of SiNW biosensors with substrate passivation (panel b) is 5.7 times faster than that of the normal SiNW biosensors (panel a). The inset shows the long-term response.

or limiting, species for the surface reaction rate. Although the antibody density should be maximized for the sensing experiment, it is more critical to maximize the local antigen concentration in the vicinity of NWs for faster detection, which supports the observations in literature^{9–11} that enhancing the mass transport of the analyte is the key to further improve the performance of NW biosensors.

We further extended our efforts in investigating simple passive mixing methods to enhance the analyte transport. Enhancing the analyte transport to the NW biosensors represents a different challenge compared to that represented by mixing two fluids in a microfluidic channel. NWs are very small, fragile, sensitive to the local flow field and wired by metal contacts for conductance measurement with the result that certain mixing strategies for microfluidics, such as the use of three-dimensional serpentine microchannels,²⁴ flow confinement,²⁵ decreased channel height,²⁶ and electrokinetics-related mixing,^{13,27} are either ineffective¹² or difficult to implement. Therefore, we proposed three simple methods: (1) device substrate passivation, (2) microfluidic channel configuration modification, and (3) suspending NW away from the bottom wall, to improve the NW sensing performance.

First, the device substrate passivation aims to remove all other possible sinks of the analyte other than NWs. The SiNW biosensors are typically fabricated on silicon substrates (Figure 3a). The NWs and substrate are both covered by SiO_2 and hence have the same surface chemical properties. Consequently, the immobilized antibodies link to both NWs and the substrate. Because the surface area of the substrate is significantly larger than that of the NWs, the substrate scavenges the scarce analyte and slows down the sensing response. When the substrate binding is blocked (Figure 3b), the complex concentration B ($t = 100$ s) is increased by a factor of 5.7 (Figure 3c). Substrate passivation can be realized by changing the substrate materials, modifying the substrate surfaces with polymers or other agents before the NW device fabrication, or confining surface functionalization to NWs only.

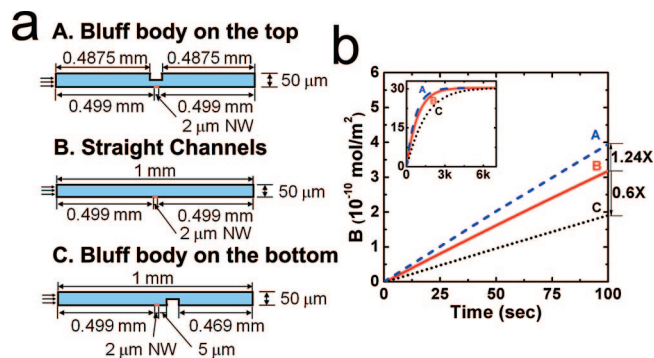


Figure 4. Effects of channel shapes on the complex formation rate. (a) Three different channel schematics (A. a bluff body on the top; B. normal straight channel; C. a bluff body on the bottom). NWs are indicated as the red line on the bottom wall in the middle of the channel. (b) The complex formation rate of the top bluff body is 1.24 times faster than that of the normal straight channel and the adverse effects are observed for the bottom bluff body downstream of the channel. The long-term response is shown in the inset. (Bluff body in A and C: $25 \mu\text{m} \times 25 \mu\text{m}$.)

Second, the mass transport of the analyte to the NW surface can be modified by changing the microfluidic channel shape. For example, when the channel height in the NW region is reduced by half by adding a bluff body (Figure 4a) to the top channel, the local average horizontal velocity is doubled which speeds up the analyte replenishment. Actually, the complex concentration $B(t = 100 \text{ s})$ is increased by 24% which is comparable to that of increasing the averaged inlet flow velocity from the current setup by 4 times (Figure 2a). The additional enhancement comes from faster diffusional transport. The induced downward velocity by the top bluff body, together with the reduced channel height, compresses the diffusion depletion zone and hence increases the analyte concentration gradient toward the NW. Consequently, the diffusional flux of the analyte to the NW is increased by the top bluff body. For the same reason, when a bluff body is added to the bottom wall after the NW (Figure 4a), the induced upward velocity expands the diffusion depletion zone resulting in a reduced diffusional flux of the analyte to the NW. Consequently, the complex concentration $B(t = 100\text{s})$ is reduced by 40% (Figure 4b). Hence, obstacles such as electrodes should be avoided or minimized downstream the NWs in the sensing experiment.

Third, both the sensing response time and the sensitivity can be improved by suspending the NWs away from the floor (Figure 5a). Suspending NWs doubles the sensing area such that the total number of bound complex B_t on a single NW, calculated by integrating the bound complex B over the $2 \mu\text{m}$ length of the NW, is doubled as shown in the inset of Figure 5b. This is a unique advantage for NW suspension compared to surface passivation and the enhanced transport, which have no impact on the ultimate sensitivity. In addition, suspension of NWs to a higher velocity region also increases the convective and diffusional fluxes of the analyte to the NW. As a result, the sensing response time is reduced as well. It is seen in Figure 5b that suspending the NW for 1 and $12.5 \mu\text{m}$ leads to 1.6 and 2.6 times faster complex formation rate for the total number of bound complex B_t ,

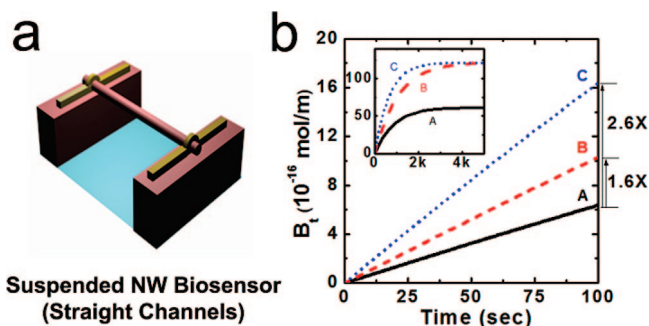


Figure 5. Effects of suspending NWs on the total number of bound complex. (a) The schematic of suspended NW biosensors in the straight channels. (b) The comparisons in terms of the formation rate of total number of bound complex (A. NWs on the floor; B. $1 \mu\text{m}$ suspended NWs; C. $12.5 \mu\text{m}$ suspended NWs). Suspending NWs improves the time response and the sensitivity as a result of the enhanced analyte transport effects and the doubled reaction surface. The inset shows the long-term response.

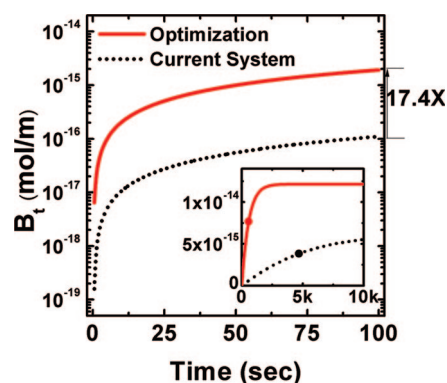


Figure 6. Comparison of optimized NW biosensors (i.e., all three designs implemented) with NWs in the typical sensing configuration shown in Figure 6. The formation rate of total number of bound complex is improved by more than 1 order of magnitude (17.4 times). If the equilibrium detection time is defined as the time when the total number of bound complex B_t approaches $(1 - e^{-1})$ of its total equilibrium value, the equilibrium detection times (the dots of the inset) for the typical and optimized systems are 4690 and 569 s, respectively (i.e., 8.2 times reduction in the detection time). The inset shows the long-term response.

respectively, than that of no suspension. The improvement for the $1 \mu\text{m}$ is less than 2 because the flow passage is confined between the bottom surface of NW and the floor. The improvement for the $12.5 \mu\text{m}$ is slightly more than 2 because the higher local convection velocity around the NW replenishes the analyte faster.

Finally, when the above three simple optimization strategies, (1) device surface passivation, (2) adding a top bluff body to the channel, and (3) suspending the NW $12.5 \mu\text{m}$ away from the floor, are implemented, the formation rate of total number of bound complex is increased by more than 1 order of magnitude (17.4 times) compared to the typical NW sensing configuration shown in Figure 6. In other words, the detection time for the NW sensor is significantly reduced. Furthermore, the detection limit indicated by the total equilibrium number of bound complex is doubled as well (inset of Figure 6).

In summary, we have numerically characterized the individual and coupled effects of convection, diffusion, and

the antigen–antibody binding reaction on the sensing performance of NW-based biosensors. For the protein sensing, the sensing response time is limited by the mass transport rate of the analyte, especially the diffusional transport process. The key to improve the sensing performance is to maximize the analyte concentration in the vicinity of the NW. Three simple optimization methods (device substrate passivation, channel configuration modification, and NW suspension) were proposed, and their combination reduced the sensing response time by more than 1 order of magnitude. Further improvement in the detection limit of NW biosensors can be realized by analyte concentrating strategies such as isotachopheresis.^{13,28}

Acknowledgment. D.R.K. acknowledges support from the Link Foundation Energy Fellowship. X.L.Z. sincerely thanks the Center of Integrated System at Stanford University for support of this work.

References

- (1) Cui, Y.; Wei, Q. Q.; Park, H. K.; Lieber, C. M. *Science* **2001**, *293* (5533), 1289–1292.
- (2) Hahm, J.; Lieber, C. M. *Nano Lett.* **2004**, *4* (1), 51–54.
- (3) Patolsky, F.; Zheng, G. F.; Hayden, O.; Lakadamyali, M.; Zhuang, X. W.; Lieber, C. M. *Proc. Natl. Acad. Sci. U.S.A.* **2004**, *101* (39), 14017–14022.
- (4) Patolsky, F.; Zheng, G.; Lieber, C. M. *Nanomedicine* **2006**, *1* (1), 51–65.
- (5) Patolsky, F.; Lieber, C. M. *Mater. Today* **2005**, *8* (5), 20–28.
- (6) Patolsky, F.; Zheng, G. F.; Lieber, C. M. *Anal. Chem.* **2006**, *78* (13), 4260–4269.
- (7) Stern, E.; Klemic, J. F.; Routenberg, D. A.; Wyrembak, P. N.; Turner-Evans, D. B.; Hamilton, A. D.; LaVan, D. A.; Fahmy, T. M.; Reed, M. A. *Nature* **2007**, *445* (7127), 519–522.
- (8) Patolsky, F.; Zheng, G. F.; Lieber, C. M. *Nat. Prot.* **2006**, *1* (4), 1711–1724.
- (9) Sheehan, P. E.; Whitman, L. J. *Nano Lett.* **2005**, *5* (4), 803–807.
- (10) Nair, P. R.; Alam, M. A. *Appl. Phys. Lett.* **2006**, *88* (23), 233120.
- (11) Zhang, W.; Stone, H. A.; Sherwood, J. D. *J. Phys. Chem.* **1996**, *100* (22), 9462–9464.
- (12) Hu, G.; Gao, Y. L.; Li, D. Q. *Biosens. Bioelectron.* **2007**, *22* (7), 1403–1409.
- (13) Sigurdson, M.; Wang, D. Z.; Meinhart, C. D. *Lab Chip* **2005**, *5* (12), 1366–1373.
- (14) Nair, P. R.; Alam, M. A. *Nano Lett.* **2008**, *8* (5), 1281–1285.
- (15) Squires, T. M.; Messinger, R. J.; Manalis, S. R. *Nat. Biotechnol.* **2008**, *26* (4), 417–426.
- (16) The following parameters were generally used for all the calculations unless mentioned: the average inlet flow velocity $u_0 = 1.7 \text{ mm s}^{-1}$, the density $\rho = 1000 \text{ kg m}^{-3}$, the dynamic viscosity $\mu = 1 \times 10^{-3} \text{ Pa s}$, the diffusion coefficient $D = 6 \times 10^{-11} \text{ m}^2 \text{ s}^{-1}$ (the diffusion coefficient of representative proteins, for example, prostate-specific antigen (PSA) or streptavidin, in water),^{17,18} and the inlet concentration $c_0 = 100 \text{ pM}$. The immobilized antibody density is $R_t = 3 \times 10^{-8} \text{ mol m}^{-2}$ (c.a., 2×10^{16} molecules/ m^2 or 1250 particles/ μm^2 of NW), which is chosen to be the average of experimental results of more than 500 particles/ μm^2 ,³ and theoretical estimation of about 2000 particles/ μm^2 .¹⁹ Note that all estimations are based on a 20 nm diameter NW. The association and dissociation rate constants k_a and k_d are $2.7 \times 10^6 \text{ M}^{-1} \text{ s}^{-1}$ and $2.4 \times 10^{-3} \text{ s}^{-1}$, respectively, based on the binding between PSA and a monoclonal antibody (mAb), and the resulting affinity constant k_a/k_d (10^9 M^{-1}) is consistent with the experimental measurement.²⁰ The effects of different k_a and k_d values under the same affinity constant on NW sensing are also investigated in the paper.
- (17) Kamholz, A. E.; Schilling, E. A.; Yager, P. *Biophys. J.* **2001**, *80* (4), 1967–1972.
- (18) Wu, G. H.; Datar, R. H.; Hansen, K. M.; Thundat, T.; Cote, R. J.; Majumdar, A. *Nat. Biotechnol.* **2001**, *19* (9), 856–860.
- (19) Eddowes, M. J. *Biosensors* **1987**, *3* (1), 1–15.
- (20) Katsamba, P. S.; Navratilova, I.; Calderon-Cacia, M.; Fan, L.; Thornton, K.; Zhu, M. D.; Vanden Bos, T.; Forte, C.; Friend, D.; Laird-Offringa, I.; Tavares, G.; Whatley, J.; Shi, E. G.; Widom, A.; Lindquist, K. C.; Klakamp, S.; Drake, A.; Bohmann, D.; Roell, M.; Rose, L.; Dorocke, J.; Roth, B.; Luginbuhl, B.; Myszyka, D. G. *Anal. Biochem.* **2006**, *352* (2), 208–221.
- (21) Our calculation predicts a detection time on the order of several thousand seconds which is longer than reported NW sensing times (on the order of one hundred seconds).^{1,22} The discrepancy may come from the uncertainties in the association and dissociation rate constants and the immobilized antibody numbers. For example, the binding reaction rates can be affected by the electrostatic interaction between charged proteins and charged surface of NWs.¹⁵ Consequently, the magnitudes of these parameters were varied over several orders in our simulations to probe a broader parameter space.
- (22) Zheng, G. F.; Patolsky, F.; Cui, Y.; Wang, W. U.; Lieber, C. M. *Nat. Biotechnol.* **2005**, *23* (10), 1294–1301.
- (23) Zimmermann, M.; Delamarche, E.; Wolf, M.; Hunziker, P. *Biomed. Microdevices* **2005**, *7* (2), 99–110.
- (24) Liu, R. H.; Stremmer, M. A.; Sharp, K. V.; Olsen, M. G.; Santiago, J. G.; Adrian, R. J.; Aref, H.; Beebe, D. J. *J. Microelectromech. Syst.* **2000**, *9* (2), 190–197.
- (25) Hofmann, O.; Voirin, G.; Niedermann, P.; Manz, A. *Anal. Chem.* **2002**, *74* (20), 5243–5250.
- (26) Brody, J. P.; Yager, P.; Goldstein, R. E.; Austin, R. H. *Biophys. J.* **1996**, *71* (6), 3430–3441.
- (27) Lin, H.; Storey, B. D.; Oddy, M. H.; Chen, C. H.; Santiago, J. G. *Phys. Fluids* **2004**, *16* (6), 1922–1935.
- (28) Jung, B. G.; Zhu, Y. G.; Santiago, J. G. *Anal. Chem.* **2007**, *79* (1), 345–349.

NL801559M